

Parallelization of the inverse fast multipole method with an application to boundary element method

Toru Takahashi^{a,*}, Chao Chen^b, Eric Darve^{b,c}

^a*Department of Mechanical Systems Engineering, Nagoya University, Furo-cho, Nagoya, Aichi, 464-8603 Japan*

^b*Institute for Computational & Mathematical Engineering, Stanford University, 496 Lomita Mall, 94305, Stanford, CA, USA*

^c*Department of Mechanical Engineering, Stanford University, 496 Lomita Mall, 94305, Stanford, CA, USA*

Abstract

We present an algorithm to parallelize the inverse fast multipole method (IFMM), which is an approximate direct solver for dense linear systems. The parallel scheme is based on a greedy coloring algorithm, where two nodes in the hierarchy with the same color are separated by at least σ nodes. We proved that when $\sigma \geq 6$, the workload associated with one color is embarrassingly parallel. However, the number of nodes in a group (color) may be small when $\sigma = 6$. Therefore, we also explored $\sigma = 3$, where a small fraction of the algorithm needs to be serialized, and the overall parallel efficiency was improved. We implemented the parallel IFMM using OpenMP for shared-memory machines. Successively, we applied it to a fast-multipole accelerated boundary element method (FMBEM) as a preconditioner, and compared its efficiency with (a) the original IFMM parallelized by linking a multi-threaded linear algebra library and (b) the commonly used parallel block-diagonal preconditioner. Our results showed that our parallel IFMM achieved at most 4 \times and 11 \times speedups over the reference method (a) and (b), respectively, in realistic examples involving more than one million variables.

Keywords: Inverse Fast Multipole Method, Parallelization, Fast Multipole Method, Boundary Element Method, Preconditioning, OpenMP

1. Introduction

We are interested in solving a large-scale dense linear system

$$Ax = b \tag{1}$$

with N unknown variables. Such systems arise from many science and engineering areas, such as discretized integral equations, boundary element methods (BEMs), machine learning, etc. To solve 1, a naive Gaussian elimination requires $O(N^3)$ computation and $O(N^2)$ memory, which is prohibitive when N is large. While an iterative solver such as CG and GMRES requires $O(N^2)$ computation and memory per iteration, the number of iterations can be large in presence of

*Corresponding author

Email address: toru.takahashi@mae.nagoya-u.ac.jp (Toru Takahashi)

ill-conditioning and indefinite problems and the $O(N^2)$ costs limit their application to truly large-scale problems. To overcome these disadvantages, the fast multipole method (FMM) [1, 2, 3, 4] can be used to accelerate the computation of matrix-vector products at every iteration of an iterative method, reducing the computation and memory costs to typically $O(N)$.

In order to further reduce the number of iterations of an iterative method, the inverse fast multipole method (IFMM) [5, 6] has been developed among various fast direct solvers [7, 8, 9, 10] and \mathcal{H} -matrix methods [11, 12]. These methods perform Gaussian elimination on a compressed representation of A and computes an approximated factorization of A with nearly linear computational cost. The IFMM is inspired and closely related to the FMM since they use the same hierarchical decomposition of the problem domain (a.k.a. the FMM tree), which corresponds to a partitioning of the unknowns in $\mathbf{1}$, and use the same far-field (multipole-to-local) and near-field (particle-to-particle) translation operators, which corresponds to the full-rank and the low-rank matrix blocks in A , respectively. This allows the IFMM to solve $\mathbf{1}$ with the same asymptotic computation and memory complexities as the FMM, i.e., $O(N \log^2 \frac{1}{\varepsilon})$, where ε is a prescribed accuracy. The efficiency of the IFMM has been studied in several previous works for solving $\mathbf{1}$: Quaife et al [13] and Coulier et al [6] applied the IFMM as preconditioners for the GMRES [14] to solve $\mathbf{1}$ from the immersed boundary method regarding Stokes flow problems in two and three dimensions (3D); Takahashi et al [15] applied the IFMM together with the low-frequency FMM to accelerate the BEM for the 3D Helmholtz equation; Coulier et al [16] applied the IFMM to reduce the cost of a mesh deformation method which is based on the radial basis function interpolation.

To further reduce the runtime of the IFMM for large problem sizes (~ 1 million variables), this paper introduces the parallel IFMM algorithm targeting at shared-memory machines. Although the IFMM uses the same hierarchical tree decomposition as the FMM, the data dependency of the IFMM is much more complicated: the work associated with nodes at the same level in the hierarchy is *not* embarrassingly parallel as it is in the upward pass and the downward pass of the FMM [17, 18]. Rather than the FMM, the data dependency in the IFMM is similar to that in the incomplete Cholesky factorization [19] but has a special structure associated with the FMM hierarchical decomposition. Rather than solving $\mathbf{1}$ directly, the IFMM solves the equivalent *extended sparse linear system* [6], which is associated with the FMM tree structure. As defined in the original FMM, every node in the FMM tree has a list of neighbors and an interaction list of nodes in the far field. In the IFMM, one step of (block) Gaussian elimination on a node in the FMM tree leads to a dense Schur complement among its neighbors (a.k.a., clique). The Schur complement is then compressed based on the low-rank structure in the FMM, which effectively updates the far-field translation operators of the neighbors and affects the nodes in the neighbors' interaction lists.

Our parallel IFMM algorithm is based on a greedy coloring algorithm (3), which assigns the same color to nodes that are apart from each other by a distance of σ . We proved that the workload for nodes in the same group (or nodes with the same color) is embarrassingly parallel when $\sigma \geq 6$, or technically speaking, the neighbors' interaction lists of a node n_1 do not intersect with the neighbors of another node n_2 if n_1 and n_2 have the same color. So we derived the basic parallel IFMM algorithm (3.2) associated with $\sigma = 6$. For the targeting problem sizes (~ 1 million), we found that the number of colors is large (the average group size is small), which limits the parallelism and leads to a significant synchronization cost.

Therefore, we derived the improved parallel IFMM algorithm (3.3) associated with $\sigma = 3$ in our coloring algorithm. With $\sigma = 3$, there exists a race condition for processing two nodes with the same color: their neighbors may need to update the same far-field translation operator.

So these updates are serialized and form a critical section in our improved parallel algorithm. Fortunately, these far-field updates account for only a small fraction of the entire computation (see Fig. 26 in [6]), and the overhead of serialization is paid back by the tremendous improvement of parallel efficiency from large group sizes and a small number of groups/colors.

In our previous study [15], a naive parallel IFMM algorithm was developed by simply replacing all matrix computations such as matrix-matrix multiplication, LU decomposition, and the SVD with their parallel counterparts in the sequential IFMM algorithm. This approach can be realized easily by linking the sequential IFMM code with a multi-threaded linear algebra library such as the Intel MKL library [20] and the OpenBLAS library [21]. However, this over-fine-grained parallelization would inevitably introduce overwhelming overhead when the number of threads is large. Another closely related approach is the distributed-memory parallel solver introduced by Chen et al [22], which parallelizes the LoRaSp algorithm [23], an analog of the IFMM for solving 1 when A is sparse.

To summarize, this paper presents parallel IFMM algorithms for solving large-scale dense linear systems, and especially, our work makes the following three main contributions:

1. analyzing the data dependency and identifying the parallelism in the sequential IFMM algorithm.
2. deriving two parallel IFMM algorithms (3.2 and 3.3) based on our coloring scheme (3).
3. reporting benchmarks and comparisons between our parallel IFMM algorithms and two existing methods for solving real-world problems involving more than a million variables.

The rest of the paper is organized as follows. 2 reviews the basics of the IFMM algorithm. 3 describes our parallel strategy and an implementation using OpenMP [24]. 4 incorporates the parallel IFMM to solve dense linear systems from the fast-multipole accelerated BEM (FMBEM) for 3D Helmholtz equation. 5 gives two numerical examples to assess the efficiency of our parallel algorithms. 6 concludes this study.

2. IFMM

In this section, we describe the sequential IFMM algorithm focusing on the data dependency there and introduce some FMM terminologies used in this paper. For more details, the readers may see the references [5, 6].

IFMM is a fast direct solver with $O(N \log^2 \frac{1}{\epsilon})$ complexity for solving a linear system $Ax = b$, where the matrix-vector product with $A \in \mathbb{R}^{N \times N}$ can be evaluated with the FMM. This type of linear system arises from various science and engineering applications. As an example, consider an electrostatic field generated by N charges, where the i -th charge is located at $\mathbf{p}_i \in \mathbb{R}^3$ and the electric potential is given as b_i at \mathbf{p}_i . We are interested in solving for the charge density x_i . This problem can be formulated as $Ax = b$, where $x := [x_1, \dots, x_N]^T$, $b := [b_1, \dots, b_N]^T$, and the (i, j) -th element of A is given by the Coulomb interaction, i.e., $\frac{x_i}{4\pi\epsilon|\mathbf{p}_i - \mathbf{p}_j|}$ if $i \neq j$ and 0 otherwise, where ϵ denotes a permittivity. To solve such a linear system, IFMM takes the following four steps.

2.1. Hierarchical domain decomposition

We carry out the standard hierarchical partitioning of the problem domain as in the FMM [2, 3, 4] and associate the partitioning with an *octree* (*quadtree*) in a three (two) dimensional space.

This partitioning can be easily parallelized with the geometric information of the problem domain. For ease of presentation, we assume the tree is *uniform* (a.k.a., *complete*), so there are $n_\kappa = 2^{\kappa d}$ nodes at level $\kappa = 0, 1, \dots, \ell$, where d is the space dimension. Based on the partitioning, we also define the *neighbors* and the *interaction list* of a tree node i as in the FMM (a partition refers to a (cubic) cluster of points in the d -dimensional space):

Neighbors: tree nodes corresponding to adjacent partitions of node i (excluding i);

Interaction list: non-adjacent partitions whose parent is a neighbor of node i 's parent.

Remark 1. *Our definition of neighbors obeys the standard definition in graph theory but differs from one in the FMM, where the neighbors of a node includes the node itself.*

2.2. Initialization of tree data structure

Given that the FMM can be used to compute matrix-vector product with A in 1, we initialize our tree data structure with the six translation operators in the FMM: P2P, P2M, L2P, M2M, M2L, and L2P. In particular, every leaf node stores all six FMM operators associated its partition, and every internal tree node stores M2M, M2L, and L2P associated with its partition (the other three operators are initially empty and will be computed in the algorithm; see lines 41 – 42 in 1). In the context of BEM, the expressions of the FMM translation operators can be found in [15]. Note this initialization step is embarrassingly parallel with respect to all tree nodes, and this was introduced in our previous work [15].

Remark 2. *From an algebraic perspective, our tree data structure corresponds to the graph of the extended sparse linear system [6] of 1 (see Figure 10 in [6]). Specifically, the extended sparse linear system is constructed through introducing auxiliary variables into 1, which are nothing but the “multipole moments” and the “local coefficients” in the FMM. These auxiliary variables satisfy relations as defined in the FMM, and solving the extended system is equivalent to solving 1. As an example, assume a three-level hierarchy in the domain decomposition, the extended sparse linear system is the following:*

$$\begin{bmatrix} P2P^{(3)} & L2L^{(3)} & & & & & \\ M2M^{(3)T} & & -I & & & & \\ & -I & M2L^{(3)} & L2L^{(2)} & & & \\ & & M2M^{(2)T} & & -I & & \\ & & & -I & M2L^{(2)} & & \end{bmatrix} \begin{Bmatrix} x^{(3)} \\ z^{(3)} \\ y^{(3)} \\ z^{(2)} \\ y^{(2)} \end{Bmatrix} = \begin{Bmatrix} b \\ 0 \\ 0 \\ 0 \\ 0 \end{Bmatrix}, \quad (2)$$

where $x^{(3)}$ are exactly the unknowns in 1, $y^{(\kappa)}$ and $z^{(\kappa)}$ are the multipole moments and the local coefficients associated with all the tree nodes at level κ , I denotes the identity matrix, and the other matrix blocks correspond to FMM translation operators at different levels.

2.3. Factorization

After initializing our tree data structure, we have effectively transformed the original $N \times N$ dense problem to a (block) sparse linear system with $O(N)$ nonzero entries. To compute an approximate factorization of the sparse matrix in linear complexity, the IFMM employs both Gaussian elimination and low-rank approximation of fill-in blocks.

The factorization phase of the IFMM is summarized in 1, which is a level-by-level traversal of the tree from the leaf level towards the root, as the upward pass in the FMM. For tree nodes at the same level, an elimination-and-compression strategy is conducted iteratively as follows.

At a node i , (block) Gaussian elimination is carried out on the associated variables (line 3), leading to fill-in blocks among its neighboring nodes (a.k.a., *clique*). Then, a compression step is carried out on all pairs of nodes that are neighbors of i (line 4). For such a pair of nodes (p, q) , the IFMM may compute a low-rank approximation of the associated fill-in block and update existing FMM operators, depending on whether p or q has been visited/eliminated and whether they are in each other's interaction list (lines 5, 8, 20 and 22). In particular, if a node q is not eliminated and p is in q 's interaction list, node q needs to update the stored M2L operators corresponding to its interaction list (lines 15 and 30). The same principle applies to node p (line 29). Finally, after level κ is traversed, the IFMM aggregates the M2M, L2L, and M2L operators of nodes that have the same parent to form the P2M, L2P, and P2P operators of their parent at level $\kappa - 1$ for $\kappa > 2$ (lines 41 and 42). When $\kappa = 2$, a dense linear system is formed with all M2L operators of the level and factorized with the standard LU factorization; this step is intentionally omitted in 1 to save space.

As the above shows, the elimination-and-compression process on a tree node involves only its neighbors and their interaction lists. So two sufficiently distant nodes at the same level can be processed in parallel, which forms the basis of our parallel algorithm in 3.

Remark 3. *Algebraically speaking, we have computed an implicit factorization of the extended sparse linear system (with $O(N)$ nonzeros), which consists of (block) triangular factors and (block) diagonal factors.*

2.4. Solve

With the (implicit) factorization, the solve phase follows the standard (sparse) forward and backward substitutions. As 2 shows, the in-place solve algorithm consists of three parts: initialization, upward traversal, and downward traversal of our tree data structure. For the initialization, every leaf node extracts corresponding elements in a given right-hand size, and every internal tree node gets a zero vector. It is obvious that this initialization can be easily parallelized among all nodes in the tree.

Both forward and backward substitutions employ the level-by-level traversal as in the factorization, and local updates on the solution vector of node i involves only the neighbors of i (lines 15 and 30). Assume two nodes i and j can be processed in parallel during the factorization, then it is easy to see that they can also be processed in parallel during the two substitutions.

Remark 4. *As in the factorization, we omit the solve with respect to the (small) linear system at level 1, which is done with standard (dense) forward and backward substitutions.*

Remark 5. *2 is a simplification of the algorithm presented in [5, 6], where the original solve algorithm involves not only $x^{(\kappa)}$ but also multipole moments $y^{(\kappa)}$ and local coefficients $z^{(\kappa)}$. The data dependency in the solve algorithm is exactly the same.*

3. Parallelization of IFMM

In this section, we describe the parallelization for each of the four steps in the IFMM. The first step — hierarchical domain decomposition — can be done using existing parallel partitioning

packages, such as Zoltan [25]. The second step — initialization of tree data structure — is embarrassingly parallel with respect to all tree nodes, and this has been introduced in our previous work [15], so we skip the details here. The last two steps — factorization and solve — are the main challenges and the focus of this section.

As hinted earlier, our parallel strategy is based on coloring: assigning colors to tree nodes at the same level such that nodes of the same color can be processed in parallel during the factorization and the solve. To be more specific, our parallel algorithm replaces the loop over all tree nodes at a level (line 2 in 1, and lines 13 and 29 in 2) with nested loops, where the outer loop goes over all colors *sequentially*, and the inner loop goes over tree nodes with the same color *in parallel*.

To that end, we introduce the separation parameter σ , which characterizes the minimum (normalized) distance between all pairs of nodes having the same color, and also serves as the constraint in our coloring algorithm. Let the partitions be cubes of size L at a level in the FMM-tree, and the normalized (infinity norm) distance between two tree nodes u and v is defined as

$$\text{dist}(u, v) := \frac{\max(|x_u - x_v|, |y_u - y_v|, |z_u - z_v|)}{L},$$

where (x_u, y_u, z_u) and (x_v, y_v, z_v) are the coordinates of the two partition (cube) centers associated with u and v , respectively. Note that by construction, $\text{dist}(u, v)$ is a non-negative integer, and

$$\text{dist}(u, v) = \begin{cases} 0 & u = v, \\ 1 & u \in \mathcal{N}_v (\Leftrightarrow v \in \mathcal{N}_u), \\ 2 \text{ or } 3 & u \in \mathcal{I}_v (\Leftrightarrow v \in \mathcal{I}_u). \end{cases} \quad (3)$$

The separation parameter, or coloring constraint is thus defined as

$$\sigma = \min \{ \text{dist}(u, v) \mid \text{color}(u) = \text{color}(v) \}, \quad (4)$$

where the function “color()” returns the color (an integer) of a node.

In the following, we analyze the data dependency in 1 and 2 and show what value σ needs to take in the coloring algorithm.

3.1. Data dependency

Suppose we have two threads T_i and $T_{i'}$, and want to process two nodes i and i' independently. Apparently, $i \neq i'$ means $\sigma \geq 1$. The data dependency in the IFMM falls into three cases as follows.

(a) Local operations

In 1 and 2, T_i (resp. $T_{i'}$) updates local data of node i (resp. i') and reads data from neighbors of i (resp. i'). For example, T_i updates the “eliminated” flag (line 3) in 1 and the “visited” flag (line 14) in 2, and reads these flags of node i ’s neighbors (1: lines 5, 8, 20 and 22, and 2: lines 16 and 31). If node i' coincides with i ’s neighbor p , the flags of i' can be updated by $T_{i'}$ while T_i is working on node i according to the original flags of $p (= i')$. This is thus a race condition. To avoid it, i and i' should not be in each other’s neighbor list, i.e., $i \notin \mathcal{N}_{i'}$ ($\Leftrightarrow i' \notin \mathcal{N}_i$). According to 3, this is guaranteed if

$$\sigma \geq 2.$$

(b) **Neighbor operations**

In 1 and 2, T_i (resp. $T_{i'}$) updates the local data of i 's (resp. i' 's) neighbors, i.e., nodes p and q (resp. p' and q'). This includes two scenarios as the following. First, T_i updates operators/data associated with a single neighbor of i , e.g., $M2M_{\tilde{q}q}$ and $L2L_{q\tilde{q}}$ (lines 16 and 32) in 1 and $x_p^{(k)}$ (line 17 and 19) in 2, where \tilde{p} denotes the parent of p . Second, T_i updates operators associated with two neighbors of i including $M2L_{pq}$, $M2L_{qp}$, $P2L_{pq}$, $M2P_{qp}$, $P2P_{pq}$, and $P2P_{qp}$ in 1.

Overall, the neighbor lists of i and i' should not overlap, i.e., $\mathcal{N}_i \cap \mathcal{N}_{i'} = \emptyset$, which is guaranteed if

$$\sigma \geq 3.$$

Remark 6. Proof of $\mathcal{N}_i \cap \mathcal{N}_{i'} = \emptyset$ when $\sigma \geq 3$: since $3 \leq \sigma \leq \text{dist}(i, i') \leq \text{dist}(i, q) + \text{dist}(q, q') + \text{dist}(q', i')$, where $q \in \mathcal{N}_i$ and $q' \in \mathcal{N}_{i'}$, we have $\text{dist}(q, q') \geq 1$, i.e., $\mathcal{N}_i \cap \mathcal{N}_{i'} = \emptyset$.

Remark 7. 1 and 2 show two examples corresponding to the above two scenarios, and illustrate that $\mathcal{N}_i \cap \mathcal{N}_{i'} \neq \emptyset$ when $\sigma = 2$, while $\mathcal{N}_i \cap \mathcal{N}_{i'} = \emptyset$ when $\sigma = 3$.

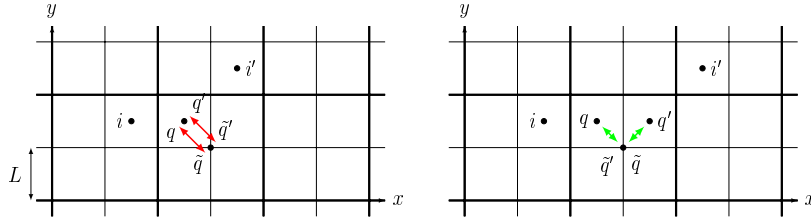


Figure 1: T_i (resp. $T_{i'}$) updates operators (arrows) associated with q and \tilde{q} (resp. q' and \tilde{q}'), where \tilde{q} (resp. \tilde{q}') is the parent, which corresponds to the center of the coarser box. (Left) When $\sigma = 2$, $q = q'$ and $\tilde{q} = \tilde{q}'$, so there is a race condition when T_i and $T_{i'}$ update the corresponding operators (red arrows) in parallel. (Right) When $\sigma = 3$, $\tilde{q} = \tilde{q}'$, but $q \neq q'$, so the corresponding operators (green arrows) can be updated in parallel.

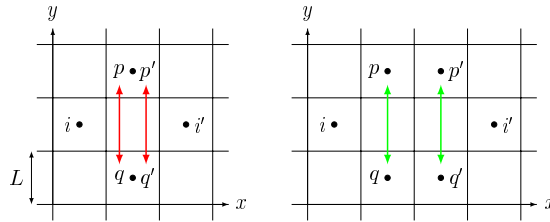


Figure 2: T_i (resp. $T_{i'}$) updates operators (arrows) associated with p and q (resp. p' and q'). (Left) When $\sigma = 2$, $p = p'$ and $q = q'$, so there is a race condition when T_i and $T_{i'}$ update the corresponding operators (red arrows) in parallel. (Right) When $\sigma = 3$, $p \neq p'$ and $q \neq q'$, so the corresponding operators (green arrows) can be updated in parallel.

(c) **Neighbors' interaction list operations**

This operation exists only in 1, not in 2. T_i (resp. $T_{i'}$) updates i 's (resp. i' 's) neighbors' interaction list (underlined lines in 1). Suppose $q \in \mathcal{N}_i$ and $q' \in \mathcal{N}_{i'}$. The condition that

$q \notin \mathcal{I}_{q'} (\Leftrightarrow q' \notin \mathcal{I}_q)$ needs to be satisfied such that there is no race condition when T_i updates \mathcal{I}_q and $T_{i'}$ updates $\mathcal{I}_{q'}$ in parallel. In other words, the parents of q and q' cannot be neighbors. This is guaranteed if

$$\sigma \geq 6.$$

Remark 8. Proof of $q \notin \mathcal{I}_{q'}$ when $\sigma \geq 6$: since $6 \leq \sigma \leq \text{dist}(i, i') \leq \text{dist}(i, q) + \text{dist}(q, q') + \text{dist}(q', i')$, where $q \in \mathcal{N}_i$ and $q' \in \mathcal{N}_{i'}$, we have $\text{dist}(q, q') \geq 4$, i.e., $q \notin \mathcal{I}_{q'}$ according to 3.

Remark 9. 3 illustrates examples that $q \in \mathcal{I}_{q'}$ when $\sigma = 5$, while $q \notin \mathcal{I}_{q'}$ when $\sigma = 6$.

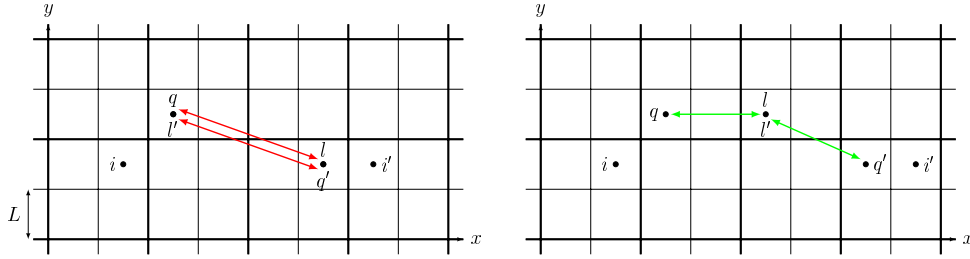


Figure 3: T_i (resp. $T_{i'}$) updates $M2L_{ql}$ (resp. $M2L_{q'l'}$) where $q \in \mathcal{N}_i, l \in \mathcal{I}_q$ (resp. $q' \in \mathcal{N}_{i'}, l' \in \mathcal{I}_{q'}$). (Left) When $\sigma = 5$, $q = l'$, and $q' = l$, so there is a race condition when T_i and $T_{i'}$ update $M2L_{ql}$ and $M2L_{q'l'}$ (red arrows), respectively, in parallel. (Right) When $\sigma = 6$, $q \neq l'$, and $q' \neq l$, so $M2L_{ql}$ and $M2L_{q'l'}$ (green arrows) can be updated in parallel.

3.2. Basic parallel algorithm ($\sigma = 6$)

As the above analysis shows, if nodes i and i' have the same color and $\sigma = 6$, two threads T_i and $T_{i'}$ have no interference with each other in processing i and i' , respectively. Therefore, we can replace the loop over nodes at the same level (line 2 in 1, and lines 13 and 29 in 2) with a double-loop over colors (in serial) and nodes that have the same color (in parallel).

Specifically, we color the tree nodes at every level subject to the constraint that $\sigma = 6$ in 4 (3 in 3.4). Suppose at level κ , there are g_κ colors, and the tree nodes fall into $G_0, G_1, \dots, G_{g_\kappa-1}$ groups according to their colors. Our basic parallel algorithm can be obtained by replacing

for Node $i = 0$ **to** $n_\kappa - 1$

at line 2 in 1 and line 13 in 2 with

for Color $I = 0$ **to** $g_\kappa - 1$
 #pragma omp parallel for
for all Node $i \in G_I$

and replacing

for Node $i = n_\kappa - 1$ **to** 0

at line 29 in 2 with

for Color $I = g_\kappa - 1$ **to** 0
 #pragma omp parallel for
for all Node $i \in G_I$

using the “parallel for” pragma in OpenMP.

Note that we have to use the same coloring (σ) in 1 and 2 because the ordering in the solve needs to be consistent with that in the factorization; in particular for solving dense linear systems, the ordering of the solve is exactly the reverse of the factorization. Therefore, we cannot apply $\sigma = 3$ for 2 despite the fact that the solve is irrelevant to the data dependency of (c).

3.3. Improved parallel algorithm ($\sigma = 3$)

To improve the efficiency of the basic parallel algorithm, we consider using a smaller σ in the coloring algorithm at the cost of serializing a part of the algorithm. However, $\sigma \leq 2$ leads to race conditions in updating neighbors’ operators and neighbors’ interaction list operators, meaning the factorization and solve are serialized entirely. So, let us consider $\sigma = 3$, in which case T_i and T_r can work independently in 2, and they interfere with each other only for neighbors’ interaction list operations in 1. Therefore, our improved parallel algorithm is based on the coloring with constraint $\sigma = 3$, and *serializes* the neighbors’ interaction list operations (underlined in 1).

Specifically, we still color the tree nodes at every level (3 in 3.4), but with the constraint that $\sigma = 3$ in 4 as apposed to the $\sigma = 6$ constraint used in the basic parallel algorithm. With the coloring results, we follow the previous parallel algorithm and replace the serial loop over nodes at every level in 1 and 2 with a double-loop, where the outer loop is over all colors in serial and the inner loop is over nodes of the same color in parallel. In addition, we serialize updating neighbors’ interaction list operators (underlined in 1) to avoid race condition. This serialization can be implemented with OpenMP locks [24] or with OpenMP’s critical constructor “#pragma omp critical”, which allows only one thread in the critical region at a time. Our implementation adopts the latter for the underlined statements in 1.

Compared with the coloring results ($\sigma = 6$) used in the basic parallel algorithm, the improved parallel algorithm would have less number of colors and larger group sizes on average for every color, which implies less synchronization cost and more concurrency. The extra serialization cost in the improved parallel algorithm is expected to be small because empirically updating neighbors’ interaction list is a small fraction of the total runtime.

3.4. Coloring algorithm

Given the tree nodes at the level κ in the FMM-tree, we want to assign colors to them so that 4 holds for a prescribed σ . The number of colors used is denoted by g_κ , and the nodes can be classified into groups $G_0, G_1, \dots, G_{g_\kappa-1}$ based on their colors.

When the FMM-tree is complete, the nodes at the same level lie on a regular grid. It is easy to see that the optimal coloring has σ^3 colors, and nodes of the same color lie on a sub-grid of stride σ , as shown in 4 (a). In general, some of the nodes may be empty and do not need to be colored. In the context of the BEM, only tree nodes corresponding to boundary elements need to be colored. Such an example is shown in 4 (b).

The idea of our greedy algorithm is as follows. We find the first node that is not empty nor colored, and we color it. Then, we try to find other nodes that can be assigned the same color. To find the next node, we first make a stride of σ and search for a non-empty and un-colored node. Once we find the second node, we make a stride of σ again and continue the search. After we have exhausted all the remaining nodes, we start over for a new color. This algorithm is shown in 3.

We note that the computational cost of 3 is $O(n_\kappa)$. Since up to σ^3 groups are created at line 7, the outer triple-loop over k_0 , j_0 , and i_0 is executed up to σ^3 times. Since each length of the loops

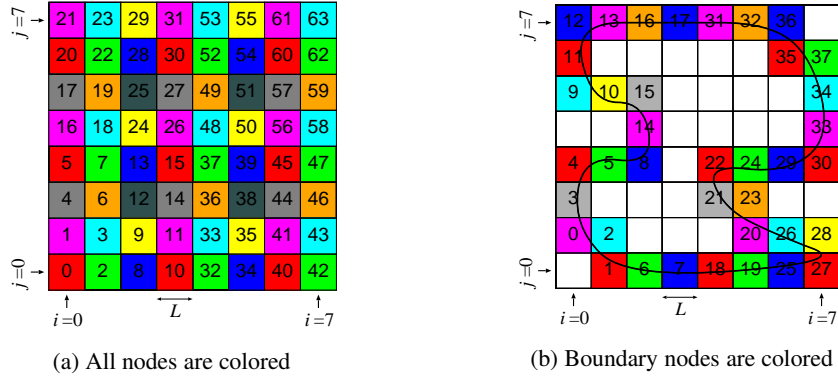


Figure 4: Coloring results of 3 in 2D for tree nodes at level $\kappa = 3$ and $\sigma = 3$. (a) The optimal coloring is achieved with $\sigma^2 = 9$ colors. Every color corresponds to a sub-grid of stride 3 in both directions. (b) Only nodes corresponding to the domain boundary are colored. $g_\kappa = 8$ colors are used.

over k , j , and i is up to $2^\kappa/\sigma$, the computational complexity is effectively $\sigma^3 \times (2^\kappa/\sigma)^3 = n_\kappa$. In fact, we observed the time to group n_κ nodes is proportional to n_κ in the two examples in 5.2 and 5.3, where $n_\kappa \lesssim 116\text{k}$. In addition, the elapsed time was less than 0.1 seconds in the case of the maximum n_κ for each example.

We also note that 3 does not guarantee to minimize the number of colors or maximize the (average) number of nodes per group. This is due to the fixed stride of σ (lines 20, 25, and 28). For example, if we look back all the nodes already colored, we would be able to find more nodes in a group but lead to more computational cost.

4. Application of IFMM to FMBEM

We apply the proposed parallel IFMM to an iterative BEM as the preconditioner. In this section, we first overview the algorithm of the BEM. Then, we define two types of the IFMM-based preconditioners, i.e., mIFMM and nIFMM. Last, we explain the standard preconditioner, that is, the leaf-based block-diagonal preconditioner and its enhancement to be compared with the IFMM-based preconditioners.

4.1. FMBEM

Following the previous study [15], we deal with the BEM for 3D Helmholtz equation. Specifically, we solve the acoustic scattering problems with the combined (or Burton-Muller type) boundary integral equations (CBIE) [26]. We use the preconditioned GMRES [27] to iteratively solve the discretized CBIE or the resulting linear system

$$Ax = b, \quad (5)$$

where $A \in \mathbb{C}^{N \times N}$ and $x, b \in \mathbb{C}^N$. Here, N stands for the number of piece-wise constant elements to discretize the surface of a given model (scatterer). To accelerate the matrix-vector product for A , we use the low-frequency FMM (LFFMM) [28, 4, 29, 30, 31, 32]. The overall algorithm of our FMBEM is described in 4.

The preconditioning is performed through 5. Specifically, the algorithm computes Mr , where M denotes a preconditioner such as $M \approx A^{-1}$ and r is a known vector at a given iteration step; therefore, computing Mr means to solve $Av = r$ approximately for v . As M , we will use nIFMM, mIFMM, and BD introduced below.

4.2. IFMM-based preconditioners: nIFMM and mIFMM

In the preconditioning routine, we refer to the preconditioner M as **IFMM-based preconditioner** if v is obtained as a part of \bar{v} that is approximately solved from the IFMM-extended sparse system $\bar{A}\bar{v} = \bar{r}$, where \bar{r} is the extended vector of a given r . To use this preconditioner, we first construct \bar{A} and then factorize it according 1 or its parallel version before starting GMRES (see lines 7 and 8 in 4). Subsequently, 2 or its parallel version is performed when the preconditioning routine is called from GMRES (see 5).

We will denote an IFMM-based preconditioner as **nIFMM** if IFMM is parallelized with respect to “n”odes according to 3.2 (where $\sigma = 6$ is employed) or 3.3 (where $\sigma = 3$). In addition, we will denote another IFMM-based preconditioner as **mIFMM** if IFMM is parallelized in the grain of individual “m”atrix operations by means of a multi-threaded linear algebra package; we actually use Intel MKL [33] through Eigen [34].

We construct the IFMM with the LFFMM; in general, we may handle the IFMM with a different FMM (e.g., the black-box FMM [35]) from the FMM for the matrix-vector product, i.e., LFFMM in this study. Although it would be simple to manipulate both LFFMMs with the same hierarchy (of boundary elements), the hierarchy of the LFFMM for the matrix-vector products employs the adaptive octree differently from the uniform octree of the IFMM (recall 2.1). Nevertheless, to share the information as much as possible, we decided that both root nodes have the same position and size. Then, the FMM operators can be shared by the nodes of both FMMs especially in upper levels (see line 7 in 4). This (irregular) combination of hierarchies was actually used in the previous work [15].

Yet, the depth of the IFMM’s hierarchy (i.e., ℓ) is not necessarily the same as that of the FMM’s hierarchy (i.e., ℓ_{FMM}), although $\ell \equiv \ell_{\text{FMM}}$ was supposed in [15]. We will determine the value of ℓ_{FMM} by a conventional manner, as described in 5.1. Meanwhile, we regard ℓ as a tunable parameter, which can affect the performance of nIFMM and mIFMM.

Basically, if we let ℓ be less than ℓ_{FMM} , we no longer perform the factorization at the omitted levels $\ell + 1$ to ℓ_{FMM} . In addition, we can handle a smaller number of nodes at level ℓ than ℓ_{FMM} . The downside is that the matrix manipulation (e.g., low-rank compression) can require more computational cost because the size of individual matrices (FMM operators) increases as ℓ decreases; this is because the size is determined by the formula in 6 in 5.1. Further, the initialization cost can become large (respectively, small) if the IFMM cannot (respectively, can) fully reuse the FMM operators, especially the P2P operators, precomputed at leaf nodes of the FMM’s hierarchy (see line 7 in 4, again).

Another parameter of nIFMM is the top level $\tau \in [2, \ell]$. Namely, the node-based parallelism is applied to level τ to ℓ , while the matrix-based parallelism is applied to level 2 to $\tau - 1$. By switching the parallelism from the node-based to the matrix-based, we can expect a higher performance at coarse (upper) levels. This is because individual matrix is larger at coarse levels than fine levels and, thus, can be processed more efficiently with multiple threads.

For conciseness, we denote the nIFMM using the parameters σ (“sep”aration), τ (“top” level), and ℓ (“bot”tom level) by **nIFMMsep σ top τ bot ℓ** or **nIFMMs σ τ b ℓ** for short. Regarding mIFMM, we use the term **mIFMMbot ℓ** or **mIFMMb ℓ** to specify the bottom level ℓ . 1

summarizes the naming scheme of the IFMM-based preconditioners as well as the (extended) block-diagonal preconditioner, which will be explained in the next section.

4.3. Block-diagonal preconditioner: *BD*

We will compare mIFMM and nIFMM with the leaf-based block-diagonal preconditioner (referred to as **BD**), which is frequently used for FMBEM [29]. The corresponding preconditioning matrix M is computed as a block-diagonal matrix consisting of the inverse of the self P2P operators (i.e., $P2P_{ii}$) in terms of leaf nodes (see 5), where the FMM that BD relies on is nothing but the LFFMM for the matrix-vector product. Each self P2P operator is LU-decomposed at the initialization stage (see 4). It should be noted that BD is fully parallelizable with respect to leaf nodes in each level in both initialization and application (preconditioning) stages.

We can improve the performance of BD by selecting its bottom level (depth), denoted by ℓ_{BD} , where we actually compute the diagonal blocks of M . If we let $\ell_{BD} < \ell_{FMM}$, the corresponding M can have a wider bandwidth and become a better approximation of A^{-1} . Then, it can reduce the number of iterations until convergence. On the other hand, the cost and memory for factorizing the individual diagonal blocks becomes more expensive at the initial stage. We denote the enhanced BD using the bottom level of ℓ_{BD} by **BDbot** ℓ_{BD} or **BDb** ℓ_{BD} .

Table 1: List of the preconditioners. The value of ℓ_{FMM} is determined as in 5.1.

Name	Name specifying parameters	
nIFMM	nIFMMsep σ toprbot ℓ or nIFMMs σ trbl (where $\sigma = 3$ or 6 and $2 \leq \tau \leq \ell \leq \ell_{FMM}$)	Applies the matrix-based parallelism to level 2 to $\tau - 1$ and the node-based parallelism to level τ to ℓ .
mIFMM	mIFMMbot ℓ or mIFMMb ℓ (where $2 \leq \ell \leq \ell_{FMM}$)	Applies the matrix-based parallelism to all the levels, i.e. 2 to ℓ .
BD	BDbot ℓ_{BD} or BDb ℓ_{BD} (where $2 \leq \ell_{BD} \leq \ell_{FMM}$)	Handles nodes at level 2 to ℓ_{BD} .

5. Numerical experiments

In comparison with mIFMM and BD, we will assess the proposed parallel IFMM-based preconditioner, i.e., nIFMM, through solving two acoustic scattering problems.

5.1. Details of GMRES, FMM, IFMM, and computers

We used the restart GMRES, i.e., GMRES(m) [27], but no restart took place in the following tests since we used a sufficiently large restart parameter m , i.e., $m = 1000$ for the IFMM-based preconditioners and $m = 3000$ for BD. The iteration was terminated when the relative residual $\|Ax - b\|_2 / \|b\|_2$ became smaller than the predefined number “ tol ”. We set 10^{-5} to tol . We note that our GMRES program is not parallelized except for the preconditioning (5) and matrix-vector

routines, which is performed by the parallelized LFFMM (see below). The parallelization can lead to the reduction of the total computation time if the number of iterations is large.

Regarding the (LF)FMM, its performance can be controlled by two parameters. The first one is the maximum number of boundary elements per leaf node, denoted by μ . Once μ is given, the depth of FMM’s octree is determined as $\ell_{\text{FMM}} (\geq 2)$. The second parameter is the precision factor δ to determine the number p of the multipole and local coefficients through the empirical formula [36]

$$p := \sqrt{3}Lk + \delta \log(\sqrt{3}Lk + \pi), \quad (6)$$

where k is a prescribed wavenumber. We set 7 to δ in all the computations. We note that the row and/or column size of an initial (uncompressed) FMM operator is typically p^2 (not p). Also, we note that our LFFMM code is parallelized with respect to the loop over nodes in each level.

The major parameter of the IFMM is the relative error ε that determines the accuracy of the low-rank compression, for which we used the randomized SVD [37]. In general, a smaller ε makes the elapsed times of factorization and solve phases longer but can reduce the number of iterations [15]. We mainly used $\varepsilon = 10^{-3}$ and considered 10^{-1} and 10^{-2} for comparison.

In the case of the first example in 5.2, we used 16 cores in a desktop PC (which consists of two Intel Xeon Gold 6134 CPUs) and 512GB memory in total. As a compiler, gcc-7.3.1 was used with the optimizing flags “-O3 -march=native -mtune=native”¹. In the second example in 5.3, we needed a much memory because of larger N and k than the first case. Therefore, we used a computing node with 3TB memory and 56 cores (in four Intel Xeon E5-4650v4 CPUs). The compiler was gcc-7.3.0 with the aforementioned flags².

5.2. Test problem — sphere model

5.2.1. Problem statement

We considered an external Neumann problem for an acoustically hard sphere (with the radius of 0.5 and the center at the origin) irradiated by a point source $f(\mathbf{x})$ at $\mathbf{s} = (0.0, 0.0, 0.8)^T$, i.e., $f(\mathbf{x}) := \exp(ik|\mathbf{x} - \mathbf{s}|)/(k|\mathbf{x} - \mathbf{s}|)$. We discretized the surface of the sphere with 1003520 triangular piece-wise constant boundary elements. The exact solution is available from the reference [38, Section 10.3.1]. In what follows, we considered $k = 4, 8, 16$, and 32.; the diameter of the sphere is about five times larger than the wavelength when $k = 32$.

5.2.2. Survey of the best BD, mIFMM, and nIFMM

First of all, we searched the best value of the parameter μ (recall 5.1) so that the total computation time of the FMBEM based on the standard BD was minimized. As a result, $\mu = 40$ was nearly the best. Then, the corresponding depth ℓ_{FMM} was 7.

Consequently, using $\mu = 40$, we surveyed the best (fastest) BD, mIFMM, and nIFMM by varying the parameters ℓ_{BD} , ℓ , and τ , where the separation parameter σ was fixed to 3 (3.3). As a result, we determined **BDbot5**, **mIFMMbot6**, and **nIFMMsep3top3bot6** as the best ones in this example. The details are described in Section 1 of the supplementary material.

¹In addition, we built the IFMM program with the Eigen’s macro “EIGEN_USE_MKL_ALL” to parallelize each matrix operation by Intel MKL [33] outside parallel regions. This actually improved the performance of the related codes.

²Since both computers are based on the NUMA architecture, we considered to bind the OpenMP threads to specific computing cores. We simply bound the i -th thread to the i -th core. This improved the timing result in practice.

2 shows the statistics of the hierarchies used in the following computations. We can observe that the number of nodes of the FMM and IFMM (in the second and fourth columns, respectively) is $\sim 4^\kappa$ at level κ , which is because the distribution of boundary elements is planar in 3D. Regarding nIFMM, the statistics of the grouping with $\sigma = 3$ is shown in the fifth to eighth columns. We can see that the group size at level κ is $\sim 4^\kappa$ in average. In addition, $p \sim \kappa^{-1}$ is observed in the ninth and tenth columns.

Table 2: Statistics of the **sphere model**. “#nodes”: number of nodes of the FMM’s adaptive octree when $\mu = 40$. “#ele/node”: average number of elements per node. “IFMM’s #node”: number of nodes of the IFMM’s uniform octree when $\mu = 40$. “#groups”: number of nIFMM’s groups when $\sigma = 3$. “Min”, “Ave”, and “Max”: minimum, average, and maximum group size. “ p^2 ”: the squared number of multipole and local coefficients. Note that this statistics is independent of the wavenumber k as well as the precision parameter ε .

Level κ	FMM		IFMM #nodes	#groups	nIFMM			p^2	
	#nodes	#ele/node			Min	Ave	Max	$k = 4$	$k = 32$
2	56	17920	56	19	2	3	8	144	1089
3	272	3689	272	26	7	10	16	100	529
4	1160	865	1160	27	8	43	70	81	256
5	4694	214	4742	27	84	176	245	64	144
6	17640	56	18488	27	305	685	973	64	100
7	58730	15	70896	27	1173	2626	3712	64	81

5.2.3. Comparison under the best setting

5 shows the speedup (in terms of the total computation time) of the best nIFMM with the best BD and mIFMM. Although the best nIFMM was slower than or comparable to the best BD for low wavenumbers, it achieved 2.2 times speedup at the largest k . It should be noted that the performance of BD can be improved by parallelizing the present GMRES program. Even if this is done successfully, the best nIFMM would remain faster than the best BD at $k = 32$; this is indicated in Tables I and III of the supplementary material.

In addition, the best nIFMM was about two times faster than the best mIFMM for any k . The drop at $k = 32$ can be explained by the fact that the performance of mIFMM can increase with k , which will be examined in 5.2.4.

5.2.4. Comparison of node- and matrix-based parallelizations

We compared the two parallel methods, using the best nIFMMsep3top3bot6 and mIFMM-bot6 in 6. The factorization phase was actually boosted by the proposed node-based parallelization. The speedup became smaller with k . This is likely due to the fact that each operator becomes larger with k and, thus, individual matrix operation can be performed more efficiently with multiple threads.

Regarding the solve phase, the node-based parallelization achieved about 12 times speedup. This significant speedup is due to the fact that the number of matrix operations involved in the solve phase is absolutely small and therefore the matrix-based parallelization has little chance to work efficiently. In addition, the parallelized solve algorithm is free from the serialization unlike the factorization phase. However, similarly to the factorization phase, the efficiency of the node-based parallelization tends to decrease with k .

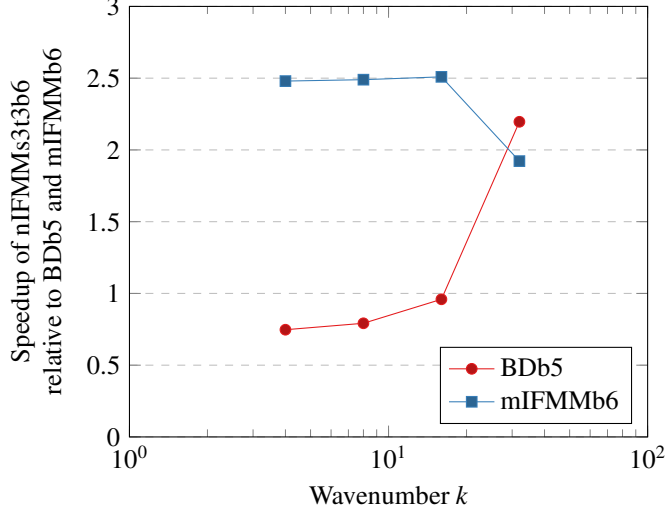


Figure 5: Speedup of the best nIFMM (i.e., nIFMMsep3top3bot6) relative to the best BD (i.e., BDbot5) and mIFMM (i.e., mIFMMbot6) in terms of the total computation time for the sphere model.

5.2.5. Influence of nIFMM's parameters

3 gives a closer look at the elapsed times of the initialization and factorization phases level by level for the best nIFMM at $k = 16$. We analyzed the influence of the parameters as follows:

1. Influence of ℓ on initialization:

To construct the extended matrix, the IFMM's initializer computes the FMM operators for every node and level (at line 7 in 4). If ℓ is chosen as ℓ_{FMM} ($= 7$), the initializer can largely reuse the operators that FMM precomputed (at line 3), although reading/writing an operator from/to memory requires $O(p^4)$ cost; this is why the initializer spent about 100 seconds even when $\ell = 7$.

If we let $\ell < \ell_{\text{FMM}}$, we no longer initialize the levels from $\ell + 1$ to ℓ_{FMM} . On the other hand, we have to newly handle the (uncompressed) FMM operators at the leaf level ℓ . The additional cost is estimated as $\sim 4^{-\ell} + 4^\ell \ell^{-4}$ from the observations³ in 5.2.2 and increases exponentially as ℓ decreases. The trade-off of the positive and negative effects can explain the trend of the initialization time in the table.

2. Influence of ℓ on factorization:

Similarly to the above observation, if we let $\ell < \ell_{\text{FMM}}$, we can omit the factorization from level $\ell + 1$ to ℓ_{FMM} . On the other hand, the time can increase as ℓ decreases, because the cost at the leaf level ℓ can be estimated as $\sim 4^\ell \times (p^2)^3 = 4^\ell \ell^{-6}$ from some presumptions⁴.

³The cost is proportional to the number of nodes and the square of the individual matrix size at the leaf level ℓ . The former is $\sim 4^\ell$, while the latter is $\sim (4^{-\ell})^2$ for $P2P_{ij}^{(\ell)}$ and $\sim (p^2)^2 \sim \ell^{-4}$ for others such as $M2L_{ij}^{(\ell)}$, where $p \sim \kappa^{-1}$ holds at level κ .

⁴The first factor 4^ℓ denotes the number of nodes at leaf level ℓ and the second factor $(p^2)^3$ denotes the cost of a matrix-matrix product, which is the typical manipulation in the factorization, at the leaf level, where uncompressed FMM operators of size $\sim p^2 \times p^2$ are manipulated

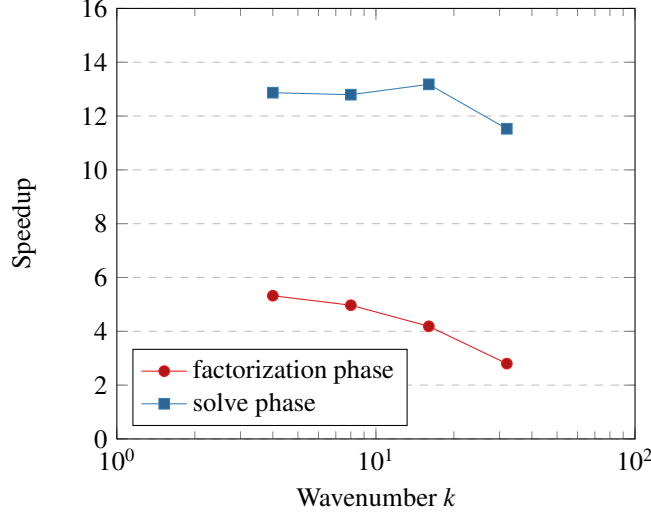


Figure 6: Speedup of the node-based parallelization relative to the matrix-based parallelization in terms of the factorization and solve phases. Here, since the number of iterations (denoted by “niter” in Tables II and III in the supplementary material) is preconditioner specific, the time of the solve phase was calculated by dividing the preconditioning time (which is spent for executing the preconditioning in 5) by the number of applications (i.e., niter + 2).

This cost function has the minimum value at $\ell = \frac{6}{\log 4} \approx 4.3$. This indicates that there exists an optimal value of ℓ that minimizes the cost at leaf level.

In fact, 3 shows that, when we decreased ℓ from 7 ($= \ell_{\text{FMM}}$) to 6, the time for the leaf level almost remained, but the total time was decreased by the time for level 7, i.e., about 47 seconds. This is the positive effect of decreasing ℓ . On the other hand, when we decreased ℓ from 6 to 5 or 4, both time for the leaf level and total time increased significantly. This corresponds to the negative effect and means that the minimizer was actually around 6 rather than 4.3.

3. Influence of τ on factorization:

In 3, $\tau = 3$ has no clear difference from $\tau = 2$ at level 2, while $\tau = 4$ certainly spoiled the performance at level 3, to which the matrix-based parallelization is applied. This is because the size of each matrix (operator) at level 3 is too small to cultivate an enough parallel efficiency with 16 computing cores.

5.2.6. Basic parallel algorithm ($\sigma = 6$) vs improved parallel algorithm ($\sigma = 3$)

We compared the improved parallel algorithm based on $\sigma = 3$ with the basic parallel algorithm based on $\sigma = 6$. The latter is free from any serialized operations, but the group size is about eight ($= 6^3/3^3$) times smaller than $\sigma = 3$ in average.

When we varied τ from 2 to 4 and ℓ from 4 to 7 in the case of $\sigma = 6$, the best performance was obtained by nIFMMsep6top4bot6, although the value of τ was almost insensitive to the timing result.

Table 3: Breakdown of the factorization and initialization times (in seconds) of nIFMM in the sphere model.

$\varepsilon = 10^{-3}, k = 16$

Precon.	Factorization								Initialization Total
	Total	Level							
		2	3	4	5	6	7		
nIFMMs3t2b7	125	6	6	9	17	40	47	100	
nIFMMs3t2b6	82	5	6	8	16	46		101	
nIFMMs3t2b5	122	4	6	9	103			435	
nIFMMs3t2b4	985	4	6	974				1844	
nIFMMs3t3b7	129	7	6	9	17	40	48	103	
nIFMMs3t3b6	81	5	6	8	16	45		102	
nIFMMs3t3b5	122	3	6	9	103			419	
nIFMMs3t3b4	979	5	6	968				1803	
nIFMMs3t4b7	132	6	11	9	17	40	48	104	
nIFMMs3t4b6	86	5	11	8	16	45		102	
nIFMMs3t4b5	126	3	10	10	104			413	
nIFMMs3t4b4	987	5	11	971				1757	

7 compares nIFMMsep6top4bot6 with nIFMMsep3top3bot6 (i.e., the best nIFMM using $\sigma = 3$). Although the difference in total computation time is not significant, this figure shows that $\sigma = 3$ was indeed better than $\sigma = 6$ for any k .

5.2.7. Influence of ε and accuracy

We tested relatively low-precision ε , i.e., $\varepsilon = 10^{-1}$ and 10^{-2} , for mIFMMbot6 and nIFMMsep3top3bot6, which are the best in the case of $\varepsilon = 10^{-3}$. A larger ε led to a shorter initialization and factorization time but resulted in a larger number of iterations. As a result, $\varepsilon = 10^{-2}$ maximized the performances of both mIFMMbot6 and nIFMMsep3top3bot6 in the sphere model.

In all the above analyses, the accuracy of the solutions obtained by all the preconditioners were almost the same for every k . In particular, ε did not affect the accuracy; this is shown in Tables I, II, and III in the supplementary material.

5.2.8. Memory consumption

Regarding the largest $k = 32$, nIFMMsep3top3bot6 required 381, 393, and 410GB for $\varepsilon = 10^{-1}$, 10^{-2} , and 10^{-3} , respectively. About 90% of the required memory was spent for constructing the extended matrix \bar{A} in the initialization phase. Since this phase is common, mIFMMbot6 required almost the same memory as the nIFMM. The huge memory consumption is problematic, but will be less of an issue with distributed memory.

On the other hand, BDbot5 required 25GB for $k = 32$, where the precomputation of M2L, P2P, and the preconditioning matrix M spent 9, 6, and 5GB, respectively.

5.3. Realistic example — office model

5.3.1. Problem statement

We consider a complicated problem in comparison with the previous one. Namely, we solve a mixed boundary value problem (BVP) where the scatterer is an office building consisting of four floors (8 left and center). Regarding the boundary condition, the Dirichlet boundary condition

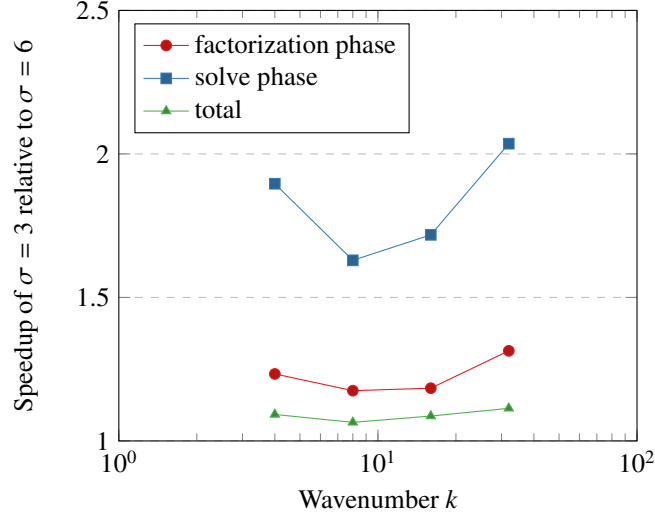


Figure 7: Speedup of the best nIFMM based on $\sigma = 3$ (i.e., nIFMMsep3top3bot6) relative to the best one based on $\sigma = 6$ (i.e., nIFMMsep6top4bot6) in the sphere model. Here, the time of the solve phase was calculated by dividing the preconditioning time by $\text{niter} + 2$; see the caption of 6.

of $u = 1$ is given as the sound source on a wall in the third floor (8 right), while the Neumann boundary condition of $q = 0$ is given everywhere else. The model is discretized with 1218200 elements.

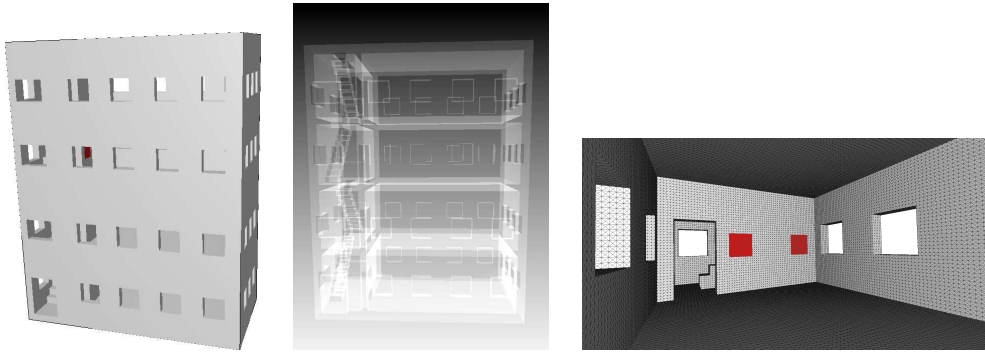


Figure 8: Office model. (Left) Outlook. The dimensions width \times depth \times height are $0.8 \times 0.4 \times 1.025$. (Center) Transparent view. (Right) Two sound sources (colored in red) on the wall in the third floor and the boundary element mesh.

We chose the maximum number of elements per node (μ) as 40, following the previous sphere model. Then, the depth of the FMM hierarchy (i.e., ℓ_{FMM}) became 7 as shown in 4.

5.3.2. Comparison under the best settings

We focus on our prime interest, that is, the performance of nIFMM over BD and mIFMM. Prior to this, we surveyed the best setting of each preconditioner; the details are described in Section 2 of the supplementary material. Basically, since the present model is more complicated,

Table 4: Statistics for the **office** model. The meanings of the headings are the same as those in 2.

Level κ	FMM		IFMM	#groups	nIFMM			p^2	
	#nodes	#ele/node	#nodes		Min	Ave	Max	$k = 4$	$k = 32$
2	32	38069	32	18	1	2	4	144	2704
3	256	4759	256	27	4	9	18	100	1156
4	1512	806	1512	27	10	56	86	81	529
5	6775	180	6775	27	76	251	347	64	256
6	28867	42	28890	26	116	1111	1512	64	144
7	65264	11	115789	19	4002	6094	9089	64	100

the number of iterations became larger than the previous model. Hence, a longer initialization time can compensate the total computation time. We actually considered $\ell_{BD} \in \{2, 7\}$, $\sigma = 3$, $\tau \in \{2, 3\}$, and $\ell \in \{4, \dots, 7\}$ for the survey.

As a result, BDbot4 was nearly the best for $k \leq 32$ and BDbot3 for $k = 64$. Meanwhile, mIFMMbot5 and nIFMMsep3top3bot5 were nearly the best for higher wavenumbers.

9 shows the speedup of nIFMMsep3top3bot5 relative to mIFMMbot5 and BD in terms of the total computation time. Here, the time of BD was chosen as the best (shortest) time of BDbot3–7 for every wavenumber; this is because it is difficult to determine the best BD for all the wavenumbers. Clearly, the nIFMM increased its performance with k and achieved about 11.4 times speedup at the largest wavenumber. Meanwhile, the speedup over the mIFMM was about 4 times.

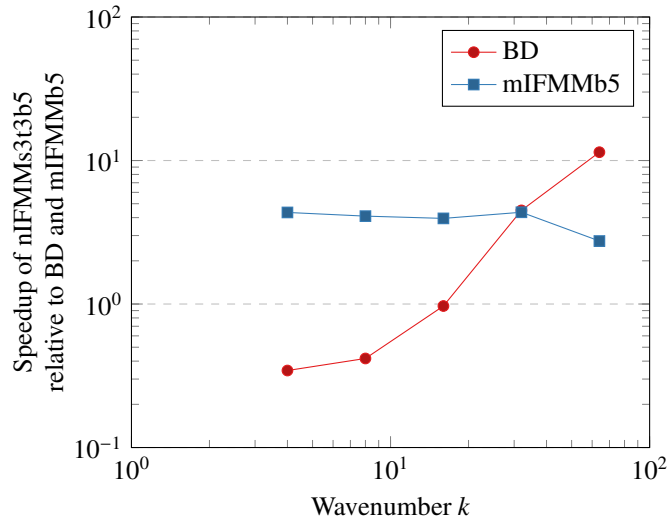


Figure 9: Speedup off the best nIFMM (i.e., nIFMMsep3top3bot5) relative to the best mIFMM (i.e., mIFMMbot5) and BD in terms of the total computation time for the **office** model.

5.3.3. Basic parallel algorithm ($\sigma = 6$) vs improved parallel algorithm ($\sigma = 3$)

We simply changed the value of σ from 3 to 6 in the best nIFMM (i.e., nIFMMsep3top3bot5). 10 shows that $\sigma = 3$ is indeed faster than $\sigma = 6$ for any wavenumbers. Similarly to the previous

example in 5.2.6, we can confirm that the serialization of a small fraction of the factorization algorithm pays the total efficiency.

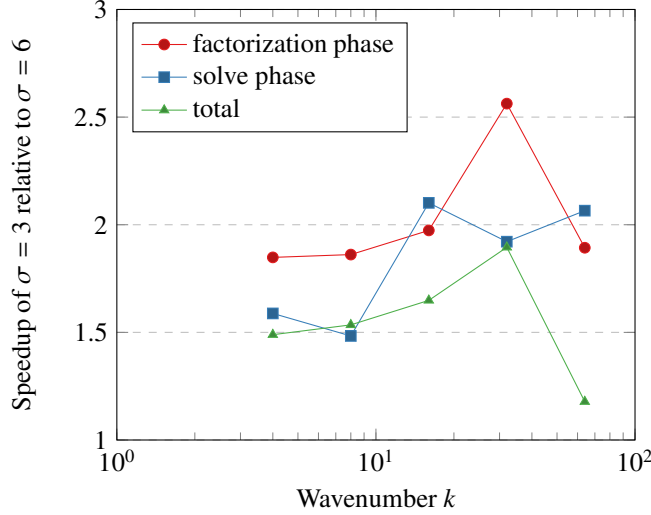


Figure 10: Speedup of nIFMMsep3top3bot5 relative to nIFMMsep6top4bot5 in the office model. The meanings of the legends are the same as those in 7.

5.3.4. Accuracy

Finally, we point out that the IFMM-based preconditioners with using larger values of ε , that is, 10^{-1} and 10^{-2} , produced inaccurate solutions in some cases, where the distribution of the sound pressure u on the boundary were erroneous at specific portions.

The previous work [15] suggested that $\varepsilon = 10^{-2}$ was a safer choice by considering the fact that the erroneous solutions were induced by $\varepsilon = 10^{-1}$ in a similar mixed BVP of $N = 147k$ and $k \leq 32$. However, this is not true for the present problem of $N = 1218k$ and $k \leq 64$. The present experiments conclude $\varepsilon = 10^{-3}$ is safer. In addition, $\varepsilon = 10^{-3}$ was faster than $\varepsilon = 10^{-1}$ and 10^{-2} for most of cases of k because $\varepsilon = 10^{-3}$ resulted in more rapid convergence.

Choosing an optimal value of the IFMM's precision parameter ε still remains an open question regardless of the parallelization.

6. Conclusion

To perform IFMM (2) efficiently, we proposed to parallelize its factorization and solve phases with respect to nodes in every level of the hierarchy. Unlike in FMM, a loop over nodes cannot be parallelized straightforwardly due to the data dependencies among nodes. To overcome it, we divide nodes in a level into groups (colors) so that any two nodes in each group are separated by σL or more, where σ is a predefined parameter (termed to separation parameter) and L denotes the edge length of the nodes (3.4). The number of groups is bounded from above by σ^3 . Then, if σ is 6 or more, we can prove that all the nodes (or computing threads assigned to them) in a group never result in any race condition and, thus, can be handled concurrently (3.1). The grouping (coloring) with $\sigma = 6$ is our basic strategy (3.2). However, the resulting number of

nodes per group is not so large especially for upper levels. The number σ should be large for a high parallel efficiency. We thus considered to use a smaller value of σ and chose the minimum value of 3 (3.3). This can increase the number of nodes per group at most 8 ($= 6^3/3^3$) times. In this case, we can still parallelize the loop over nodes by serializing a small fraction of the factorization. We implemented a parallel IFMM code with OpenMP, which can run on a shared memory machine.

In the later part of this paper, we applied the parallel IFMM to a fast iterative BEM, which can be used for 3D acoustic scattering problems, as the preconditioner (4). The numerical results in 5 confirmed that the preconditioner based on the proposed “n”ode-based parallelization (termed to **nIFMM**) was indeed faster than the “m”atrix-based parallelization (termed to **mIFMM**). Also, nIFMM outperformed the extended block-diagonal preconditioner (termed to **BD**) for relatively large wavenumbers. Here, the numbers of unknowns are about one million and the size of scatterer is up to ten times wavelength.

In these performance comparisons, we optimized the bottom level (depth) of the hierarchy (i.e., ℓ for both nIFMM and mIFMM and ℓ_{BD} for BD), which can be chosen differently from the FMM’s hierarchy (i.e., ℓ_{FMM}). We discussed the tendency of the timing result due to ℓ , but a way to predetermine an optimal choice has not been established yet. Regarding nIFMM, we also investigated the separation parameter σ and the top level τ as the tunable parameters. We found that τ was not so influential to the timing result, while we observed that $\sigma = 3$ was indeed better than $\sigma = 6$.

Finally, we remark the future directions of this study:

- First, in order to make full use of threads, we will realize the nested parallelization, that is, parallelize each matrix operation in the parallelized loop over nodes. This is not allowed by the current version of Eigen [34], which is used as the front-end of the MKL. This can be regarded as a hybrid of the node- and matrix-based parallelizations, which are alternative in a level in this study. Such a fine (and complicated) control of threads would be possible by utilizing both Intel MKL [33] and OpenMP [24] (without Eigen) but technically challenging.
- Second, we will implement a parallel IFMM code for memory-distributed systems, using a message passing interface (MPI). This parallelization could resolve the issue of huge memory consumption, which we experienced on shared-memory systems. For this regard, the parallelization proposed for a sparse direct solver (LoRaSp [23]) by Chen et al [22] would be helpful. However, the modification to dense systems is not trivial because the algorithm of IFMM is significantly different from that of LoRaSp. Once this parallelization using MPI is done, it could be combined with the proposed (or the aforementioned nested) parallelization using OpenMP to construct a so-called MPI-OpenMP hybrid parallelization, which is a good fit for modern cluster computing systems.

Acknowledgments

The work of the first author is partially supported by JSPS KAKENHI under Grant Number 18K11335.

Part of this research was done at Stanford University. This material is based upon the work supported by the Department of Energy under Award Number DE-NA0002373-1.

Some of the computing for this project was performed on the Sherlock cluster 2.0. We would like to thank Stanford University and the Stanford Research Computing Center for providing computational resources and support that contributed to these research results.

References

- [1] V. Rokhlin, Rapid solution of integral equations of classical potential theory, *Journal of Computational Physics* 60 (2) (1985) 187–207.
- [2] L. Greengard, V. Rokhlin, A fast algorithm for particle simulations, *Journal of Computational Physics* 73 (2) (1987) 325–348.
- [3] E. Darve, The fast multipole method: Numerical implementation, *Journal of Computational Physics* 160 (1) (2000) 195–240.
- [4] N. Nishimura, Fast multipole accelerated boundary integral equation methods, *Applied Mechanics Reviews* 55 (4) (2002) 299–324.
- [5] S. Ambikasaran, E. Darve, The inverse fast multipole method, *ArXiv e-prints* [arXiv:1407.1572](https://arxiv.org/abs/1407.1572).
- [6] P. Coulier, H. Pouransari, E. Darve, The inverse fast multipole method: Using a fast approximate direct solver as a preconditioner for dense linear systems, *SIAM Journal on Scientific Computing* 39 (3) (2017) A761–A796.
- [7] P. Martinsson, V. Rokhlin, A fast direct solver for boundary integral equations in two dimensions, *Journal of Computational Physics* 205 (1) (2005) 1–23.
- [8] E. Corona, P.-G. Martinsson, D. Zorin, An direct solver for integral equations on the plane, *Applied and Computational Harmonic Analysis* 38 (2) (2015) 284–317.
- [9] J. Bremer, A. Gillman, P.-G. Martinsson, A high-order accurate accelerated direct solver for acoustic scattering from surfaces, *BIT Numerical Mathematics* 55 (2) (2015) 367–397.
- [10] K. L. Ho, L. Ying, Hierarchical interpolative factorization for elliptic operators: Differential equations, *Communications on Pure and Applied Mathematics* 69 (8) (2016) 1415–1451.
- [11] M. Bebendorf, *Hierarchical Matrices: A Means to Efficiently Solve Elliptic Boundary Value Problems*, Lecture Notes in Computational Science and Engineering, Springer Berlin Heidelberg, 2008.
- [12] L. Banjai, W. Hackbusch, Hierarchical matrix techniques for low- and high-frequency Helmholtz problems, *IMA Journal of Numerical Analysis* 28 (1) (2008) 46–79.
- [13] B. Quaife, P. Coulier, E. Darve, An efficient preconditioner for the fast simulation of a 2D Stokes flow in porous media, *International Journal for Numerical Methods in Engineering* 113 (4) (2018) 561–580.
URL <https://onlinelibrary.wiley.com/doi/abs/10.1002/nme.5626>
- [14] Y. Saad, M. H. Schultz, Gmres: A generalized minimal residual algorithm for solving nonsymmetric linear systems, *SIAM Journal on scientific and statistical computing* 7 (3) (1986) 856–869.
- [15] T. Takahashi, P. Coulier, E. Darve, Application of the inverse fast multipole method as a preconditioner in a 3D Helmholtz boundary element method, *Journal of Computational Physics* 341 (2017) 406–428.
URL <http://www.sciencedirect.com/science/article/pii/S0021999117302875>
- [16] P. Coulier, E. Darve, Efficient mesh deformation based on radial basis function interpolation by means of the inverse fast multipole method, *Computer Methods in Applied Mechanics and Engineering* 308 (2016) 286–309.
- [17] E. Darve, C. Cecka, T. Takahashi, The fast multipole method on parallel clusters, multicore processors, and graphics processing units, *Comptes Rendus Mecanique* 339 (2-3) (2011) 185–193.
- [18] R. Yokota, J. P. Bardhan, M. G. Knepley, L. Barba, T. Hamada, Biomolecular electrostatics using a fast multipole BEM on up to 512 GPUs and a billion unknowns, *Computer Physics Communications* 182 (6) (2011) 1272 – 1283.
- [19] Y. Saad, *Iterative methods for sparse linear systems*, pws pub, Co., Boston.
- [20] E. Wang, Q. Zhang, B. Shen, G. Zhang, X. Lu, Q. Wu, Y. Wang, Intel math kernel library, in: *High-Performance Computing on the Intel® Xeon Phi™*, Springer, 2014, pp. 167–188.
- [21] OpenBLAS.
URL <https://github.com/xianyi/OpenBLAS>
- [22] C. Chen, H. Pouransari, S. Rajamanickam, E. G. Boman, E. Darve, A distributed-memory hierarchical solver for general sparse linear systems, *Parallel Computing* 74 (2018) 49–64.
URL <http://www.sciencedirect.com/science/article/pii/S0167819117302077>
- [23] H. Pouransari, P. Coulier, E. Darve, Fast hierarchical solvers for sparse matrices using extended sparsification and low-rank approximation, *SIAM Journal on Scientific Computing* 39 (3) (2017) A797–A830.
URL <https://doi.org/10.1137/15M1046939>
- [24] The OpenMP API Specification for Parallel Programming.
URL <http://openmp.org/wp>

- [25] E. G. Boman, U. V. Catalyurek, C. Chevalier, K. D. Devine, The Zoltan and Isorropia parallel toolkits for combinatorial scientific computing: Partitioning, ordering, and coloring, *Scientific Programming* 20 (2) (2012) 129–150.
- [26] A. J. Burton, G. F. Miller, The application of integral equation methods to the numerical solution of some exterior boundary-value problems, *Proceedings of the Royal Society of London A: Mathematical, Physical and Engineering Sciences* 323 (1553) (1971) 201–210.
- [27] Y. Saad, *Iterative Methods for Sparse Linear Systems*, 2nd Edition, Society for Industrial and Applied Mathematics, Philadelphia, PA, USA, 2003.
- [28] M. A. Epton, B. Dembart, Multipole translation theory for the three-dimensional Laplace and Helmholtz equations, *SIAM J. Sci. Comput.* 16 (4) (1995) 865–897.
- [29] Y. Liu, *Fast Multipole Boundary Element Method: Theory and Applications in Engineering*, Cambridge University Press, Cambridge, 2009.
- [30] Y. J. Liu, S. Mukherjee, N. Nishimura, M. Schanz, W. Ye, A. Sutradhar, E. Pan, N. A. Dumont, A. Frangi, A. Saez, Recent advances and emerging applications of the boundary element method, *Applied Mechanics Reviews* 64 (3) (2011) 030802.
- [31] T. Takahashi, Y. Shimba, H. Isakari, T. Matsumoto, An efficient blocking M2L translation for low-frequency fast multipole method in three dimensions, *Computer Physics Communications* 202 (2016) 151–164.
- [32] E. Darve, P. Havé, Efficient fast multipole method for low-frequency scattering, *Journal of Computational Physics* 197 (1) (2004) 341–363.
- [33] Intel Math Kernel Library (Intel MKL).
URL <https://software.intel.com/en-us/intel-mkl>
- [34] G. Guennebaud, B. Jacob, et al., Eigen v3, <http://eigen.tuxfamily.org> (2010).
- [35] W. Fong, E. Darve, The black-box fast multipole method, *Journal of Computational Physics* 228 (2009) 8712–8725.
- [36] R. Coifman, V. Rokhlin, S. Wandzura, The fast multipole method for the wave equation: A pedestrian prescription, *Antennas and Propagation Magazine, IEEE* 35 (3) (1993) 7–12.
- [37] N. Halko, P. G. Martinsson, J. A. Tropp, Finding structure with randomness: Probabilistic algorithms for constructing approximate matrix decompositions, *SIAM Review* 53 (2) (2011) 217–288.
- [38] J. J. Bowman, T. B. A. Senior, P. L. E. Uslenghi, *Electromagnetic and Acoustic Scattering by Simple Shapes* (Revised edition), Hemisphere Publishing Corp., New York, 1987.

Algorithm 1 Sequential factorization algorithm. Notations: \mathcal{N}_i and \mathcal{I}_i stand for the *neighbors* and the *interaction list* of node i , respectively; \bar{p}, \bar{q} denote the parents of node p and node q , respectively; an FMM operator is denoted as A_{pq} , where A represents the operator name, and p and q stand for the *target* and *source* node [5], respectively. Underlined are the critical sections (in 3.3), and comments in orange show the data dependencies (a)–(c) in 3.1.

```

1: for Level  $\kappa = \ell$  to 2 do
2:   for Node  $i = 0$  to  $n_\kappa - 1$  do
3:     Factorize  $P2P_{ii}$  and “eliminate” node  $i$  // (a); local and neighbors of  $i$ 
4:     for all Pair  $(p, q)$ , where  $p, q \in \mathcal{N}_i$  do
5:       if Node  $p$  is eliminated & node  $q$  is eliminated then
6:         // Case 1
7:         Calculate and add fill-in blocks to  $M2L_{pq}$  and  $M2L_{qp}$  // (b); local of  $p$  and  $q$ 
8:       else if Node  $p$  is eliminated & node  $q$  is not eliminated then
9:         // Case 2
10:        Calculate fill-in blocks  $P2L'_{pq}$  and  $M2P'_{qp}$  // (b); local of  $p$  and  $q$ 
11:        if Node  $p \in \mathcal{I}_q$  then
12:          Compress fill-in  $P2L'_{pq} \approx M2L'_{pq}P2M'_{qq}$  // (b); local of  $q$ 
13:          Compress fill-in  $M2P'_{qp} \approx L2P'_{qq}M2L'_{qp}$  // (b); local of  $p$ 
14:          Update  $P2M_{qq}$  and  $L2P_{qq}$  // (b); local of  $q$ 
15:          Update  $M2L_{iq}$  and  $M2L_{qi}$  for  $l \in \mathcal{I}_p$  // local and interaction list of  $q$ 
16:          Update  $M2M_{\bar{q}\bar{q}}$  and  $L2L_{\bar{q}\bar{q}}$  // (b); local of  $q$ 
17:        else
18:          Add fill-in blocks to  $P2L_{pq}$  and  $M2P_{qp}$  // (b); local of  $p$  and  $q$ 
19:        end if
20:      else if Node  $p$  is not eliminated & node  $q$  is eliminated then
21:        // Case 3: reverse  $p$  and  $q$  in Case 2 (skipped)
22:      else if Node  $p$  is not eliminated & node  $q$  is not eliminated then
23:        // Case 4
24:        Calculate fill-in blocks  $P2P'_{pq}$  and  $P2P'_{qp}$  // (b); local of  $p$  and  $q$ 
25:        if Node  $p \in \mathcal{I}_q$  then
26:          Compress fill-in  $P2P'_{pq} \approx L2P'_{pp}M2L'_{pq}P2M'_{qq}$  // (b); local of  $q$ 
27:          Compress fill-in  $P2P'_{qp} \approx L2P'_{qq}M2L'_{qp}P2M'_{pp}$  // (b); local of  $p$ 
28:          Update  $P2M_{pp}$ ,  $L2P_{pp}$ ,  $P2M_{qq}$ , and  $L2P_{qq}$  // (b); local of  $p$  and local of  $q$ 
29:          Update  $M2L_{ip}$  and  $M2L_{pi}$  for  $l \in \mathcal{I}_p$  // (b) and (c); local and interaction list of  $p$ 
30:          Update  $M2L_{iq}$  and  $M2L_{qi}$  for  $l \in \mathcal{I}_q$  // (b) and (c); local and interaction list of  $q$ 
31:          Update  $M2M_{\bar{p}\bar{p}}$  and  $L2L_{\bar{p}\bar{p}}$  // (b); local of  $p$ 
32:          Update  $M2M_{\bar{q}\bar{q}}$  and  $L2L_{\bar{q}\bar{q}}$  // (b); local of  $q$ 
33:        else
34:          Add fill-in blocks to  $P2P_{pq}$  and  $P2P_{qp}$  // (b); local of  $p$  and  $q$ 
35:        end if
36:      end if
37:    end for
38:  end for
39:  if  $\kappa > 2$  then
40:    for Node  $i = 0$  to  $n_{\kappa-1} - 1$  do
41:      Aggregate M2M and L2L from children to form P2M and L2P. // (a); local of  $i$ 
42:      Aggregate M2L from children to form P2P. // (a); local and neighbors of  $i$ 
43:    end for
44:  end if
45: end for

```

Algorithm 2 Sequential (in-place) solve algorithm. Input: right-hand side b ; output: solution x ($\equiv x^{(\ell)}$). Notations: \mathcal{N}_i and \mathcal{C}_i stand for the *neighbors* and *children* of node i . Comments in orange show the data dependencies (a) and (b) in 3.1; there is no dependency of (c).

```

1: // Initialize node vector
2: for Level  $\kappa = \ell$  to 2 do
3:   for Node  $i = 0$  to  $n_\kappa - 1$  do
4:     if  $\kappa == \ell$  then
5:        $x_i^{(\kappa)} = b_i$  // corresponding components in the RHS vector  $b$ 
6:     else
7:        $x_i^{(\kappa)} = 0$ 
8:     end if
9:   end for
10: end for
11: // (column-oriented) forward substitution/upward pass
12: for Level  $\kappa = \ell$  to 2 do
13:   for Node  $i = 0$  to  $n_\kappa - 1$  do
14:     Mark node  $i$  as "visited" // (a); local of  $i$ 
15:     for all Node  $p \in \mathcal{N}_i$  do
16:       if Node  $p$  is visited then
17:          $x_p^{(\kappa)} - = P2L_{pi}x_i^{(\kappa)}$  // (b); local of  $p$ 
18:       else
19:          $x_p^{(\kappa)} - = P2P_{pi}x_i^{(\kappa)}$  // (b); local of  $p$ 
20:       end if
21:     end for
22:   end for
23:   for Node  $i = 0$  to  $n_{\kappa-1} - 1$  do
24:     Aggregate  $x_{\mathcal{C}_i}^{(\kappa)}$  to form  $x_i^{(\kappa-1)}$  // (a); local of  $i$ 
25:   end for
26: end for
27: // (row-oriented) backward substitution/downward pass
28: for Level  $\kappa = 2$  to  $\ell$  do
29:   for Node  $i = n_\kappa - 1$  to 0 do
30:     for all Node  $p \in \mathcal{N}_i$  do
31:       if Node  $p$  is visited then
32:          $x_i^{(\kappa)} - = M2P_{ip}x_p^{(\kappa)}$  // (a); local of  $i$ 
33:       else
34:          $x_i^{(\kappa)} - = P2P_{ip}x_p^{(\kappa)}$  // (a); local of  $i$ 
35:       end if
36:     end for
37:     Solve  $x_i^{(\kappa)}$  with the local factorization of  $P2P_{ii}$  // (a); local of  $i$ 
38:     Mark node  $i$  as "un-visited" // (a); local of  $i$ 
39:     Split  $x_i^{(\kappa)}$  into  $x_{\mathcal{C}_i}^{(\kappa+1)}$  // (a); local of  $\mathcal{C}_i$ 
40:   end for
41: end for

```

Algorithm 3 Coloring algorithm. Input: all tree nodes at level κ ; output: color of every node and the number of colors g_κ . Notation: $m = 2^\kappa$ is the number of nodes at each dimension. Based on colors, nodes can be classified into g_κ groups $G_0, G_1, \dots, G_{g_\kappa-1}$.

```

1: Initialize the first color  $g_\kappa = 0$ .
2: for  $k_0 = 0$  to  $m - 1$  do
3:   for  $j_0 = 0$  to  $m - 1$  do
4:     for  $i_0 = 0$  to  $m - 1$  do
5:       Denote the  $(i_0, j_0, k_0)$ -th node as  $u$ .
6:       if  $u$  is not empty &  $u$  is not colored then
7:         Assign color  $g_\kappa$  to node  $u$ . //  $u$  is the first node with color  $g_\kappa$ 
8:          $j\_stride = true, k\_stride = true$  // next node is at least one stride away
9:          $k = k_0$ 
10:        // check if node  $(i, j, k)$  can be colored  $g_\kappa$ 
11:        while  $k < m$  do
12:          if  $k == k_0$  then  $j = j_0$  else  $j = 0$  end if
13:          while  $j < m$  do
14:            if  $j == j_0$  &  $k == k_0$  then  $i = i_0 + \sigma$  else  $i = 0$  end if
15:            while  $i < m$  do
16:              Denote the  $(i, j, k)$ -th node as  $v$ .
17:              if  $v$  is not empty &  $v$  is not colored then
18:                Assign color  $g_\kappa$  to node  $v$ .
19:                // next node is at least one stride away
20:                 $i = i + \sigma, j\_stride = true, k\_stride = true$ 
21:              else
22:                 $i = i + 1$ 
23:              end if //  $v$ 
24:            end while //  $i$ 
25:            if  $j\_stride == true$  then  $j = j + \sigma$  else  $j = j + 1$  end if
26:             $j\_stride = false$ 
27:          end while //  $j$ 
28:          if  $k\_stride == true$  then  $k = k + \sigma$  else  $k = k + 1$  end if
29:           $k\_stride = false$ 
30:        end while //  $k$ 
31:         $g_\kappa = g_\kappa + 1$ 
32:      end if //  $u$ 
33:    end for //  $i_0$ 
34:  end for //  $j_0$ 
35: end for //  $k_0$ 

```

Algorithm 4 FMBEM using the preconditioned GMRES.

- 1: Input a boundary element mesh, boundary conditions, parameters, etc.
 - 2: Build an FMM's adaptive octree with a depth ℓ_{FMM} ; specifically, see 5.1.
 - 3: Precompute all the FMM operators, viz., P2M, M2M, M2L, L2L, L2P, and P2P.
 - 4: Compute the RHS vector b in 5 by the matrix-vector product routine.
 - 5: **if** mIFMM or nIFMM is used **then**
 - 6: Perform the hierarchical domain decomposition (2.1), which builds a uniform octree with a depth ℓ .
 - 7: Initialize the tree data structure (2.2), which constructs the extended sparse matrix \bar{A} of A in 5 with partially utilizing the FMM operators stored at line 3.
 - 8: Factorize \bar{A} according to 1.
 - 9: **else if** BD is used **then**
 - 10: Precompute the LU factorization of the self P2P operators, i.e., $P2P_{ii}$, for every leaf node i (in terms of the adaptive octree). This computation is fully parallelized with respect to i .
 - 11: **end if**
 - 12: Perform GMRES to solve 5 with the initial guess of $x = 0$.
 - 13: Output the solution x .
-

Algorithm 5 Preconditioning routine to solve $M^{-1}v = r$ for v when a vector r is given.

- 1: **if** mIFMM or nIFMM is used **then**
 - 2: Solve the extended sparse system according to 2, where the input vector b and the output vector x are regarded as r and v , respectively.
 - 3: **else if** BD is used **then**
 - 4: Solve v_i from $P2P_{ii}v_i = r_i$ with the precomputed LU factorization of $P2P_{ii}$ for every leaf node i at level ℓ_{BD} , where v_i and r_i denote the part of v and r regarding i , respectively. This computation is fully parallelized with respect to i .
 - 5: **end if**
 - 6: **return** v .
-